

Doping effects and spin correlations in C_{60} : An unrestricted Hartree-Fock study

Miguel A. Ojeda and J. Dorantes-Dávila

Instituto de Física, Universidad Autónoma de San Luis Potosí, Alvaro Obregón 64, 78000 San Luis Potosí, Mexico

G. M. Pastor

*Laboratoire de Physique Quantique, Unité Mixte de Recherche 5626 du CNRS, Université Paul Sabatier,
118 route de Narbonne, F-31062 Toulouse, France*

(Received 8 December 1998; revised manuscript received 4 May 1999)

The π -bonded system of doped C_{60} is studied in the framework of the Hubbard model using the fully unrestricted Hartree-Fock (UHF) approximation, which allows noncollinear arrangements of local-spin polarizations. Ground-state properties of a single C_{60} molecule, such as density distribution, local-spin polarizations, and spin-spin correlation functions, are determined as a function of Coulomb repulsion strength U/t and for electron or hole dopings δ close to half-band filling ($|\delta| \leq 3$). For $U > U_c$ ($U_c/t = 2.5-3.0$) the competition between nearest-neighbor antiferromagnetic spin correlations and frustrations on pentagonal loops leads to remarkable noncollinear spin arrangements, which depend sensitively on δ and U/t . For a single extra particle (electron or hole) and $U > U_c$, the charge imbalance tends to concentrate with increasing U/t along one bond connecting two pentagons. At these atoms the antiparallel spin correlations are considerably weakened. Two extra particles tend to localize at opposite poles of the C_{60} sphere. Doping-induced changes in the noncollinear spin arrangements are analyzed. Goals and limitations of the UHF calculations are discussed by comparing them with exact numerical results in the case of a cage-like 12-atom cluster. [S0163-1829(99)04431-8]

I. INTRODUCTION

The discovery of fullerene structures and the novel physical properties derived from their topology and curvature have motivated a remarkable interest in studying these complex systems.¹ Particular attention has been dedicated to alkali-metal-doped materials that exhibit superconductivity (e.g., K_3C_{60} and Rb_3C_{60}).² Understanding the physical properties of a single, eventually doped, C_{60} molecule is fundamental for the characterization of these systems. Moreover, it is generally expected that most of the basic physics behind their novel superconducting and optical properties can be captured at the scale of an individual molecular constituent. In this context, the Hubbard model has been used to determine low-energy properties of C_{60} , which derive from the outermost half-filled π -electron cloud, particularly in order to support a purely electronic mechanism for superconductivity.³⁻⁵ The spin-density distribution of the π system on the buckyball structure has been analyzed in a series of recent papers.⁶⁻¹¹ Coffey and Trugman⁶ determined the ground-state spin configuration using a classical antiferromagnetic (AF) Heisenberg Hamiltonian that corresponds to the limit of strong-Coulomb repulsion U/t in the Hubbard model. They found that the lowest-energy spin structure shows a nontrivial noncollinear spin order. This arrangement of spins minimizes AF frustrations within each pentagonal ring keeping strong AF short-range order between nearest-neighbor (NN) pentagons.⁶ In following works, the same spin structure was investigated by means of Hubbard or Pariser-Parr-Pople Hamiltonians at half-band filling, taking into account on-site and inter-site Coulomb interactions within the unrestricted Hartree-Fock (UHF) approximation.⁸⁻¹¹ A common main result of these investigations is the presence of a magnetic instability for a critical value U_c

of the on-site Coulomb repulsion. The considered magnetic structure is the one that minimizes the energy of the classical AF Heisenberg model. Monte Carlo simulations on C_{60} at half-band filling¹² and exact diagonalization studies of cage-like C_{12} (Ref. 7) support the existence of nonvanishing short-range spin correlations. Nevertheless, it should be recalled that there is no experimental evidence for a spontaneous symmetry breaking. Instead, the spin-density-wave instability calculated in the framework of the UHF approximation should be interpreted as an indication of fluctuating spin-spin correlations.

The purpose of this paper is to extend the previous investigations by varying the concentration n of π electrons away from half-band filling ($n = 1$). Extending the studies of the Hubbard model on the buckyball topology to $n \neq 1$ appears to be particularly interesting since most of the relevant properties of C_{60} -based materials, for example superconductivity, arise upon doping. In the following, we determine the ground-state properties of C_{60} by using the Hubbard model and the most general unrestricted Hartree-Fock approximation, which imposes no symmetry constraints, neither to the size and orientation of the local-spin polarizations nor to local charge densities. The best single-Slater-determinant approximation to the ground state is obtained according to the criterion of minimal energy. In this way, three-dimensional (noncollinear) spin arrangements, density redistributions, and their interplay are investigated on the same level.

II. METHOD

We consider the Hubbard Hamiltonian

$$H = -t \sum_{\langle lm \rangle \sigma} c_{l\sigma}^\dagger c_{m\sigma} + U \sum_l n_{l\uparrow} n_{l\downarrow} \quad (2.1)$$

for the π electrons in the C_{60} structure. In the usual notation, $c_{l\sigma}^\dagger$ ($c_{l\sigma}$) refers to the creation (annihilation) operator of an electron with spin σ at site l , and $n_{l\sigma} = c_{l\sigma}^\dagger c_{l\sigma}$ is the corresponding number operator. The parameters t and U denote, respectively, the NN hopping integral and the on-site Coulomb repulsion. The sum in the first term runs over all bonds that connect pentagons and hexagons. For simplicity, we neglect the difference in the hopping integrals on pentagonal and hexagonal rings ($1 \leq t_1/t_2 \leq 1.3$).¹³

In the unrestricted Hartree-Fock approximation H is replaced by the single-particle Hamiltonian

$$H_{\text{UHF}} = -t \sum_{\langle lm \rangle \sigma} c_{l\sigma}^\dagger c_{m\sigma} + U \sum_{l\sigma} (\rho_{l\sigma, l\sigma} c_{l\sigma}^\dagger c_{l\sigma} - \rho_{l\sigma, l\bar{\sigma}} c_{l\sigma}^\dagger c_{l\bar{\sigma}}), \quad (2.2)$$

from which a single-determinant approximation $|\text{UHF}\rangle$ to the ground state is obtained. In Eq. (2.2), $\rho_{l\sigma, l\sigma'}$ are the matrix elements $\rho_{l\sigma, l\sigma'} = \langle c_{l\sigma}^\dagger c_{l\sigma'} \rangle$ of the density matrix, where $\langle \dots \rangle = \langle \text{UHF} | \dots | \text{UHF} \rangle$ implies self-consistency.¹⁴ The distribution of the electron density is given by

$$\langle n_l \rangle = \rho_{l\uparrow, l\uparrow} + \rho_{l\downarrow, l\downarrow}, \quad (2.3)$$

and the spin polarization $\langle \vec{S}_l \rangle = (S_l^x, S_l^y, S_l^z)$ by

$$\begin{aligned} \langle S_l^x \rangle &= (\rho_{l\uparrow, l\downarrow} + \rho_{l\downarrow, l\uparrow})/2, \\ \langle S_l^y \rangle &= -i(\rho_{l\uparrow, l\downarrow} - \rho_{l\downarrow, l\uparrow})/2, \end{aligned} \quad (2.4)$$

$$\langle S_l^z \rangle = (\rho_{l\uparrow, l\uparrow} - \rho_{l\downarrow, l\downarrow})/2.$$

Notice that the local magnetic moments $\langle \vec{S}_l \rangle$ are collinear if and only if $\rho_{l\sigma, l\bar{\sigma}} = 0$, $\forall l$. In practice, several random spin arrangements are proposed for each U/t as starting points of the self-consistent procedure, in order to ensure that the final result corresponds to the true UHF ground state. This is important particularly for doped clusters where the spin structure cannot be inferred from the classical Heisenberg model.⁶⁻⁸ In addition, the different types of self-consistent solutions are followed as a function of U/t by small increments ΔU . In case of multiple solutions for a given U/t the UHF energies are compared.

The UHF energy can be rewritten as

$$E_{\text{UHF}} = -t \sum_{\langle l, m \rangle, \sigma} \rho_{l\sigma, m\sigma} + \frac{U}{4} \sum_l \langle n_l \rangle^2 - U \sum_l |\langle \vec{S}_l \rangle|^2. \quad (2.5)$$

One observes that the Hartree-Fock Coulomb energy E_C^{HF} —the sum of the second and third terms in Eq. (2.5)—favors a uniform density distribution and the formation of local moments $\langle \vec{S}_l \rangle$. Due to the local character of Hubbard's Coulomb interaction, the relative orientation of different $\langle \vec{S}_l \rangle$ does not affect E_C^{HF} . It is, therefore, the optimization of the kinetic energy that eventually leads to the formation of complex magnetic structures with $|\langle \vec{S}_l \rangle \cdot \langle \vec{S}_m \rangle| \neq 1$ or to nonuniform density distributions $\langle n_l \rangle$.

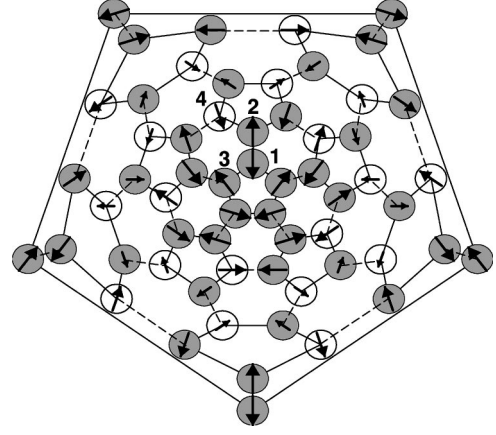


FIG. 1. Illustration of the distribution of local-spin polarizations $\langle \vec{S}_l \rangle$ in undoped C_{60} ($\delta=0$) as obtained by using the Hubbard model with $U/t=3.4$ in the fully unrestricted Hartree-Fock approximation. The three-dimensional buckyball has been mapped onto a plane in order to ease the visualization. The radius of the circle on each atomic site l is proportional to $|\langle \vec{S}_l \rangle|$. The arrows represent the projection of $\langle \vec{S}_l \rangle$ onto the xy plane, which is the plane containing the outermost pentagon. Shaded circles (open circles) indicate that the perpendicular component $\langle S_l^z \rangle$ is positive (negative). The value of $|\langle S_l^z \rangle|$ can be inferred by comparing the in-plane projection given by the arrows with the radius of the corresponding circle that is proportional to $|\langle \vec{S}_l \rangle|$. Notice that the spins are antiparallel in all bonds joining two pentagons.

III. RESULTS

The model is characterized by the dimensionless parameter U/t and by the doping $\delta = \nu - 60$, where ν is the number of π electrons. In the following, we consider values of $U/t \leq 6$ and dopings up to 3 electrons or holes ($|\delta| \leq 3$). Commonly accepted values of U/t for C_{60} correspond to the intermediate regime $2 \leq U/t \leq 5$.⁸⁻¹²

Before considering the more complicated doped cases, it is worth to recall the main results for half-band filling.⁸⁻¹¹ The local charge-density distribution $\langle n_l \rangle$ obtained within the UHF approximation is uniform for all values of $U/t \geq 0$ ($\langle n_l \rangle = 1$, $\forall l$). For $U/t \leq U_c/t \approx 2.7$ there are no spin polarizations, while for $U > U_c$ the lowest-energy solution corresponds to the noncollinear AF-like spin order illustrated in Fig. 1. The present fully unrestricted calculations confirm, as expected, the magnetic order obtained in Ref. 6. All the local spin polarizations $\langle \vec{S}_l \rangle$ of a given pentagon are coplanar matching the spin order found in an isolated pentagon with one electron per site. The angle between two NN $\langle \vec{S}_l \rangle$ in each pentagon is $4\pi/5$, which amounts to split one parallel-spin frustration among the 5 bonds. In the C_{60} buckyball, the planes containing the spins of different pentagons are arranged in such a way that the bonds connecting pentagons have antiparallel spins. Once the magnetic order sets in for $U > U_c$, the local magnetic moments increase monotonously with U/t .⁸

In the case of doped C_{60} , the optimization of the kinetic energy yields, for $U/t < U_c$, an essentially homogeneous distribution of the local charge densities that is qualitatively not far from the undoped case. For example, as shown in Fig. 2, $|\Delta n_l| \leq 0.025$ for $\delta = \pm 1$, where $\Delta n_l = \langle n_l \rangle - 1$. It is interest-

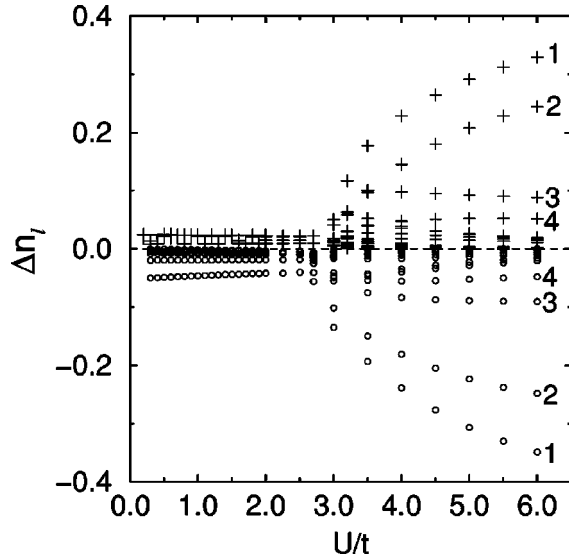


FIG. 2. Density distribution $\Delta n_l = \langle n_l \rangle - 1$ in doped C_{60} as a function of the Coulomb repulsion U/t . Positive values (crosses) and negative values (dots) refer to $\delta=1$ and $\delta=-1$, respectively. Each point for a given U/t corresponds to a different atom. The numbers refer to the atoms l illustrated in Fig. 1.

ing to note the presence of small spin polarizations already at very small values of U/t that are a consequence of degeneracies in the single-particle (SP) spectrum. For example, for $|\delta|=2$ ($|\delta|=3$) the total spin moment is $\langle S_z \rangle = 1$ ($\langle S_z \rangle = 3/2$). The associated small local moments $\langle S_i^z \rangle$ are collinear and their spatial distribution follows the small variations of the local charge density, since the majority-spin density is close to $1/2$ ($\langle S_i^z \rangle \approx |\langle n_l \rangle - 1|/2$). The situation corresponds to a full spin polarization of the carriers occupying a degenerate SP energy level and can be interpreted by applying Hund's first rule for atomic shells to the SP spectrum of the cluster.¹⁵ A similar behavior is often observed in exact diagonalization studies on smaller clusters.¹⁶ In a cage-like C_{12} cluster (truncated tetrahedron) with $\delta=-2$ ($\nu=12+\delta$) we find that the exact ground-state spin is $S=1$ already for arbitrary small $U>0$. However in other cases, for example for $\delta=2$ in C_{12} , more complex correlations result in a minimal total spin despite the presence of SP degeneracies at the Fermi energy ($S=0$ at least for $U/t \leq 16$).

The UHF results for doped C_{60} clusters change qualitatively for $U > U_c$ ($U_c/t \approx 2.7$) since a charge-density wave (CDW) and a noncollinear spin-density wave start to develop with increasing U/t . As shown in Fig. 2 for $\delta = \pm 1$, the extra-carrier density Δn_l (electron or hole) tends to localize mainly on a single bond connecting two pentagons ($l=1$ and 2) and also on the atoms of its immediate environment ($l=3$ and 4). In the rest of the atoms no significant charge transfer is observed. The redistributions of the charge density allow to reduce the Hartree-Fock (HF) energy and reflect the tendency to preserve AF-like correlations upon doping, particularly as U/t increases. However, the obtained strong charge localization is expected to be an artifact of mean field, which attempts to mimic correlation effects with a single-determinant wave function. The development of CDW's in UHF is favored by the degeneracies in the SP spectrum. For example, the charge localization at sites $l=1$ and 2 is

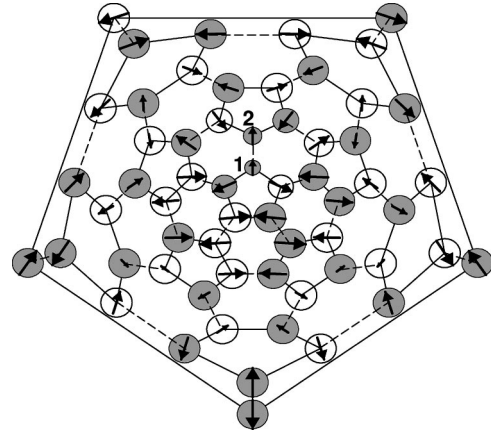


FIG. 3. Unrestricted Hartree-Fock spin distribution in single-hole doped C_{60} ($\delta=-1$) for $U/t=3.4$ (see the caption of Fig. 1). The hole is mainly localized on the atoms 1 and 2, which show small $|\langle \vec{S}_i \rangle|$ (i.e., small radii). Notice the parallel alignment of $\langle \vec{S}_1 \rangle$ and $\langle \vec{S}_2 \rangle$. Away from these sites antiparallel ordering of $\langle \vec{S}_i \rangle$ (both in-plane and off-plane components) is observed at nearest-neighbor bonds connecting pentagons (dashed-lines) as in the undoped case.

slightly larger for $\delta=-1$, which corresponds to a fivefold degenerate level in C_{60} , than for $\delta=1$ (threefold degenerate). Similar trends are found in UHF calculations on the C_{12} cluster. Moreover, the CDW instability suggests a possible orbital degeneracy of the exact ground state. In fact, exact Lanczos calculations on doped C_{12} clusters ($\delta = \pm 1$) show somewhat inhomogeneous spin-density distributions, at least as long as the point-group symmetry of the cluster is not taken explicitly into account (e.g., $\langle n_l \rangle = 13/12 \pm 0.07$ for $U/t=5$ and $\delta=1$). This indicates the presence of a ground-state orbital degeneracy that is not related to spin. The inhomogeneous density distribution results from linear combinations of the underlying symmetry adapted eigenstates. In these cases a Jahn-Teller distortion is expected. Comparison between UHF and exact results for C_{12} shows that UHF exaggerates the variations of $\langle n_l \rangle$ within the cluster (typically, $\Delta n_l \leq 0.3$ in UHF and $\Delta n_l \leq 0.07$ in symmetry unrestricted Lanczos calculations). In some cases ($\delta=2$) UHF yields an inhomogeneous density even if the corresponding exact ground state is nondegenerate and with uniform density. This limitation could be removed by restoring the cluster symmetry using linear combinations of the various broken-symmetry UHF solutions.¹⁷

For U larger than a critical value U_c , a noncollinear spin solution always yields the lowest energy. The values of U_c obtained for $1 \leq |\delta| \leq 3$ ($U_c/t = 2.6-3.0$) are not very different from U_c in the undoped case. The arrangements of spins corresponding to $\delta \neq 0$ and $U/t=3.4$ are illustrated in Figs. 3-6. The spin structures in electron- and hole-doped C_{60} are qualitatively similar. Notice, for example for $\delta = \pm 1$, the reduction of the magnitude of the spin polarization $|\langle \vec{S}_i \rangle|$ that occurs mainly on one bond connecting two pentagons ($l=1$ and 2), and the parallel alignment of the corresponding spin vectors $\langle \vec{S}_i \rangle$. Away from the sites in which the charge imbalance is localized, the spin structure resembles that of the undoped case. However, the differences become more and more important as δ increases (compare Figs. 3-6). For $\delta = \pm 2$ the hole or electron density Δn_l tends to localize at

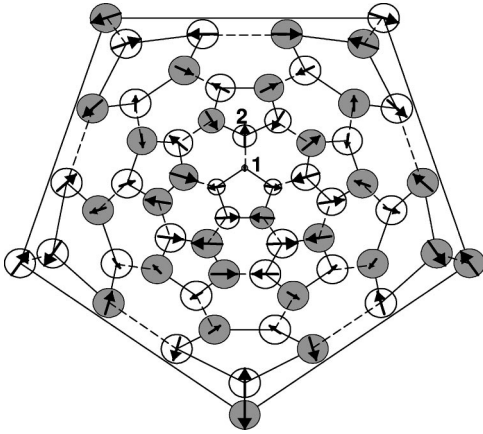


FIG. 4. Distribution of local-spin polarization $\langle \vec{S}_i \rangle$ in single-electron doped C_{60} ($\delta=1$) for $U/t=3.4$, illustrated as in Fig. 1. Notice the small value of $|\langle \vec{S}_i \rangle|$ at sites 1 and 2 where the extra electron is mainly localized.

bonds that are at opposite poles of the C_{60} sphere, namely, at the sites labeled $l=1,2$ and $m=1',2'$ in Figs. 5 and 6. The presence of two extra particles complicates the description of the spin structure, though some symmetry still remains in the charge and spin distributions. For $\delta=\pm 2$, Δn_l and $|\langle \vec{S}_l \rangle|$ are both symmetric around each hole but, in contrast to $\delta=\pm 1$, the spins at the bonds that contain most of the charge imbalance are not fully parallel ($\theta_{12}=\theta_{1'2'}\approx 25^\circ$ where $\cos \theta_{lm}=\langle \vec{S}_l \rangle \cdot \langle \vec{S}_m \rangle / |\langle \vec{S}_l \rangle| |\langle \vec{S}_m \rangle|$). The angles θ_{lm} between the spin polarizations at the rest of the bonds connecting pentagons differ only very slightly from π (typically $\cos \theta_{lm}\approx -0.999$). Quite generally, one observes an increasing collinearity of spins polarizations as compared to the single carrier case. The same trend holds for $\delta=\pm 3$. For instance, while for 1 or 2 extra holes the spin structure is three dimensional, adding one more hole ($\delta=-3$) results in a coplanar two-dimensional spin arrangement.

A more detailed understanding of the magnetic behavior is obtained by comparing the spin correlations $\langle \vec{S}_l \cdot \vec{S}_m \rangle$ as a function of doping and U/t . For half-band filling ($\delta=0$) the AF spin correlations between bonds connecting pentagons are strongest. In the UHF approximation the symmetry of the

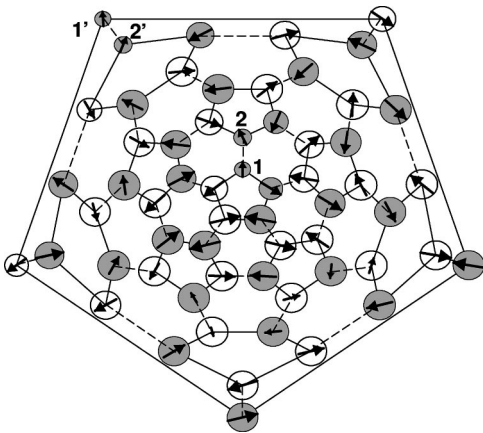


FIG. 5. Distribution of local-spin polarization $\langle \vec{S}_i \rangle$ in doped C_{60} for the case of two extra holes ($\delta=-2$, $U/t=3.4$).

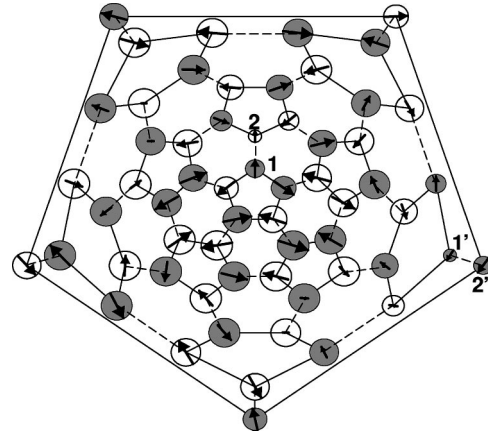


FIG. 6. Distribution of local polarization $\langle \vec{S}_i \rangle$ in doped C_{60} for the case of two extra electrons ($\delta=2$, $U/t=3.4$).

density distribution $\langle n_l \rangle$ is broken upon doping and the spin correlations between different NN's are not all the same. The average γ of $\langle \vec{S}_l \cdot \vec{S}_m \rangle$ over all bonds connecting pentagons is shown in Fig. 7. As expected, the strength of the NN antiferromagnetic spin correlations increases with U/t as we approach the Heisenberg or t - J limit. On the other side, increasing $|\delta|$ tends to break the AF order and reduces $|\gamma|$. Notice that the later effect is somewhat more important for electron doping ($\delta>0$) than for holes ($\delta<0$). These differences originate in the lack of electron-hole symmetry and in

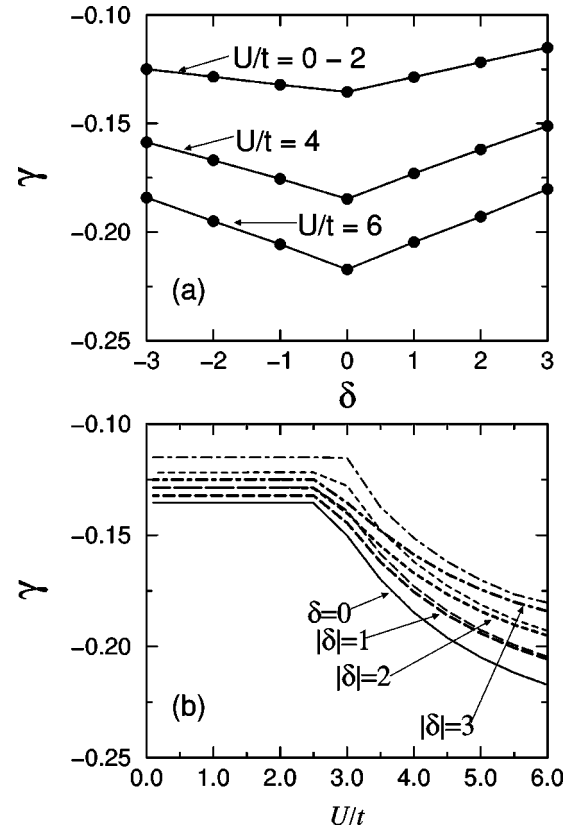


FIG. 7. Average spin correlation function $\gamma = \frac{1}{30} \sum_{lm} \langle \vec{S}_l \cdot \vec{S}_m \rangle$ between NN atoms connecting two pentagons as a function of (a) doping δ and (b) Coulomb repulsion strength U/t . The total number of π electrons is $\nu=60+\delta$.

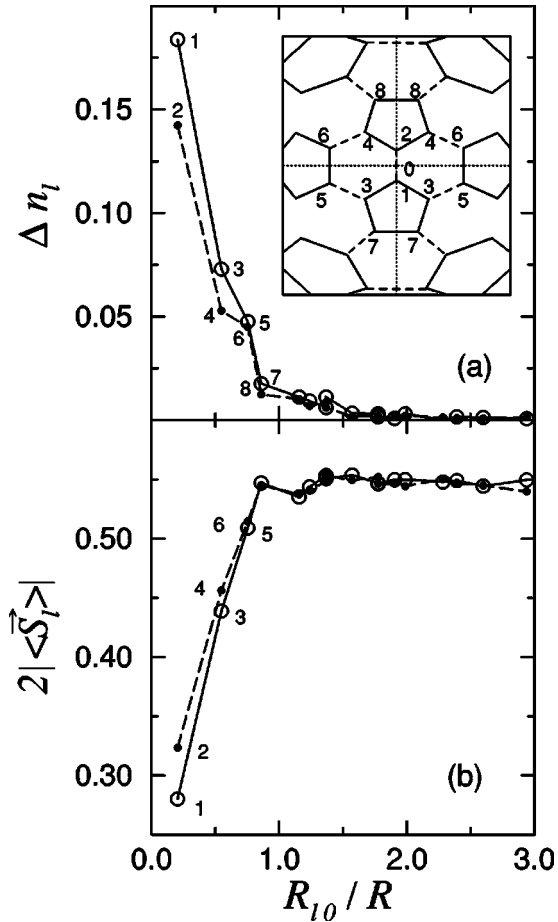


FIG. 8. Spin and charge distribution in single-hole doped C_{60} ($\delta = -1$). (a) Hole density $\Delta n_l = 1 - \langle n_l \rangle$ ($\sum_l \Delta n_l = 1$) and (b) spin polarization $|\langle \vec{S}_l \rangle|$ as a function of the distance R_{l0} between atom l and the origin 0 shown in the inset. R_{l0} is measured along the surface of the sphere of radius R containing all atoms ($R_{l0} = R\theta_l$). The lattice structure around the bond where the hole is mainly localized is illustrated in the inset. The numbers label different nonequivalent atoms l . Even and odd l are used to distinguish upper and down hemispheres. R_{l0} increases nonmonotonically with l . Full lines (odd l) and dashed lines (even l) are a guide to the eye.

the resulting asymmetry of the SP spectrum of the nonbipartite C_{60} structure. For $\delta > 0$ there is a threefold degenerate SP level at the Fermi energy, while for $\delta < 0$ the SP open shell is fivefold degenerate. This indicates that the larger the degeneracy of SP levels, the smaller the reduction of $|\gamma|$ upon doping. The trend, which is also found in exact and UHF calculations on a cage-like 12-atom cluster, can be qualitatively understood as a consequence of the larger flexibility of the carrier states with increasing degeneracy at the Fermi energy.

The angles θ_{lm} between the spin polarizations provide further insight into the complex magnetic order above U_c/t . Taking for example the case of a single hole ($\delta = -1$), we find that $\cos \theta_{lm} \approx -1$ for all but one bond connecting pentagons ($l=1$ and $m=2$ in Fig. 8) for which $\cos \theta_{12} = 1$. In other words, this one bond shows a ferromagnetic-like ordering with very small local-spin polarizations $|\langle \vec{S}_l \rangle|$. Similar trends are also observed for electron doping ($\delta = 1$). The parallel alignment of $\langle \vec{S}_l \rangle$ ($l=1,2$) and the reduction of $|\langle \vec{S}_l \rangle|$

are related to the redistribution of the extra hole or electron density Δn_l . This is shown in Fig. 8 where Δn_l and $|\langle \vec{S}_l \rangle|$ for $\delta = -1$ are given as a function of the distance R_{l0} between atom l and the bond 1-2. The charge imbalance is found predominantly on the bond with parallel spins (atoms 1 and 2). Within this bond, the average hole density is somehow asymmetrical and the local-spin polarization is larger at atom 2, which has the smaller hole concentration Δn_l . Notice that the main deviations from the undoped case ($\delta = 0$) are localized on the pentagonal and hexagonal rings surrounding bond 1-2 (up to $l \approx 8$).

IV. DISCUSSION

The symmetry breaking implied by noncollinear spin arrangements or by charge localization in finite systems is certainly an artifact of the Hartree-Fock approximation. It is therefore of considerable interest to assess the validity of the UHF results for the magnetic properties (e.g., the spin-correlation functions $\langle \vec{S}_l \cdot \vec{S}_m \rangle$) by comparing them with exact calculations on smaller clusters with similar structures. We have considered the cage-like C_{12} cluster (truncated tetrahedron) for $|\delta| \leq 2$ ($\nu = 12 + \delta$) and performed both UHF self-consistent calculations and Lanczos exact diagonalizations.¹⁸

The UHF results on C_{12} have many qualitative features in common with those on C_{60} . For $\delta = 0$ the self-consistent local-charge density is uniform for all U/t . There are no local-spin polarizations until U/t reaches the value $U_c/t \approx 2.7$. For $U > U_c$ the lowest energy UHF solution shows a noncollinear three-dimensional spin arrangement with local moments $\langle \vec{S}_l \rangle$ that increase monotonically with U . As in C_{60} , the relative orientation of the $\langle \vec{S}_l \rangle$ is independent of U ($U > U_c$) and corresponds to the one that minimizes the energy of the classical AF Heisenberg model. The $\langle \vec{S}_l \rangle$ are coplanar within each triangle, pointing along the medians as if the triangle were isolated ($\theta_{lm} = 2\pi/3$). The spin polarizations at bonds connecting two triangles are exactly antiparallel ($\theta_{lm} = \pi$). In the exact calculations for $\delta = 0$ the charge-density distribution is also uniform but there is neither a discontinuous change of behavior at a critical U/t nor permanent spin polarizations ($\langle n_l \rangle = \langle n_l \rangle = 1/2$, $\forall l$). As expected, the AF correlations increase progressively, starting at arbitrary small U .

In doped C_{12} clusters, UHF yields an approximately uniform distribution of the charge density $\langle n_l \rangle$ for $U < U_c$ ($U_c \approx 2.7$). As already discussed in Sec. III, small spin polarizations are obtained at very small U/t due to degeneracies in the SP spectrum. This is in agreement with the exact calculations for $\delta = -2$ (ground-state spin $S = 1$) but not for $\delta = 2$ ($S = 0$). For $U > U_c$ UHF yields a mixed spin and charge-density wave ($\delta \neq 0$). As in the buckyball, doping reduces AF correlations by tilting the $\langle \vec{S}_l \rangle$ away from the least frustrated solution of the classical AF Heisenberg model. While the density distribution is not uniform, the tendency to localize the extra-carrier density is weaker than in C_{60} , at least for $U/t < 6$. A representative example is illustrated in Fig. 9 for $\delta = 1$. The extra-electron density is mainly found on one triangle ($l = 1-3$ in Fig. 9) where the local moments are small and parallel to each other. As already

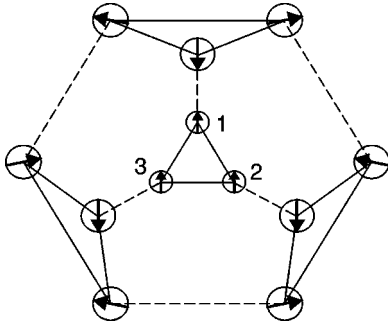


FIG. 9. Distribution of local-spin polarization $\langle \vec{S}_i \rangle$ in single-electron doped C_{12} ($\delta=1$) for $U/t=5$ (see the caption of Fig. 1). All the $\langle \vec{S}_i \rangle$ lie within the plane of the figure. Notice the smaller value of $|\langle \vec{S}_i \rangle|$ at the atoms $l=1-3$ where most of the extra-electron density is found.

noted, the Lanczos calculations also present a somewhat inhomogeneous spin-density distribution, which results from a degeneracy of the ground state. Comparison between exact and mean-field calculations for C_{12} shows, however, that UHF exaggerates the variations of $\langle n_l \rangle$ within the cluster.

A more detailed analysis of the magnetic behavior is obtained by comparing the spin correlation functions $\langle \vec{S}_l \cdot \vec{S}_m \rangle$. In Fig. 10 $\langle \vec{S}_l \cdot \vec{S}_m \rangle$ is given as a function of the intersite separation $|l-m|$ ($U/t=5$). The exact results in the undoped case ($\delta=0$) present strong antiferromagnetic spin correlations for NN sites ($|l-m|=1$) which strength decreases rapidly showing some oscillations as $|l-m|$ increases. In the inset results are given for electron and hole doping. These correspond to the cluster average γ_{lm} of $\langle \vec{S}_l \cdot \vec{S}_m \rangle$ since, as already discussed, the calculated charge distributions are in general inhomogeneous. Doping does not change the behavior qualitatively, the main effect being an overall reduction of $|\gamma_{lm}|$. Although there are appreciable quantitative differences between UHF and Lanczos results—mainly at short distances where UHF tends to underestimate the strength of AF correlations—one observes that mean field reproduces correctly the main trends in the distance dependence of $\langle \vec{S}_l \cdot \vec{S}_m \rangle$ for both undoped and doped cases ($\delta=\pm 1$). This indicates, in spite of the drawbacks resulting from symmetry breaking, that the physical picture obtained from the noncollinear-spin calculations is qualitatively correct. UHF seems a reasonable starting point for studying spin correlations in fullerene-like clusters.

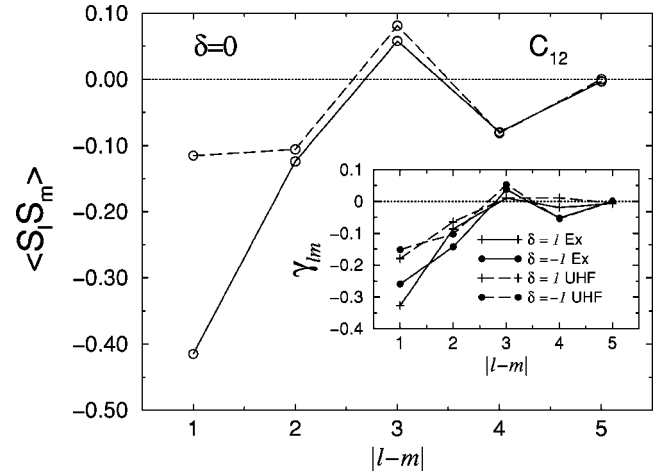


FIG. 10. Spin correlation functions $\langle \vec{S}_l \cdot \vec{S}_m \rangle$ of the single-band Hubbard model with $U/t=5$ on a cagelike C_{12} cluster (truncated tetrahedron). The number of electrons is $\nu=12+\delta$ with $\delta=0$ (main figure, circles), $\delta=1$ (inset, crosses), and $\delta=-1$ (inset, dots). Solid lines (dashed lines) refer to exact (unrestricted Hartree-Fock) calculations. For $\delta \neq 0$ results are given for the cluster averages γ_{lm} as in Fig. 7, since the charge distribution is in general not uniform.

Summarizing, the ground-state electronic properties of doped C_{60} have been studied in the framework of the Hubbard model using the fully unrestricted Hartree-Fock approximation. Complex arrangements of spin polarizations were obtained for $U/t > 2.5-3.0$ as a result of the interplay between NN antiferromagnetic spin correlations, partial localization of the extra electron or hole densities and frustration effects in the fullerene topology. Comparison with exact calculations on smaller clusters shows that UHF provides a satisfactory description of the spin correlations among π electrons in cagelike structures. It is therefore expected, in spite of the limitations of mean field, that the results reported in this paper are relevant to the physics of doped C_{60} and that noncollinear HF is a useful approach to fullerene-based materials. The present study should be also of interest from the more general perspective of noncollinear magnetism in compact frustrated structures.

ACKNOWLEDGMENTS

This work was supported by CONACyT (Mexico) and CNRS (France). M.A.O. acknowledges support from CONACyT (Mexico), and G.M.P. from the J. S. Guggenheim Memorial Foundation.

¹H. W. Kroto, J. R. Heath, S. C. O'Brien, R. F. Curl, and R. E. Smalley, *Nature (London)* **318**, 162 (1985); W. Krätschmer, L. D. Lamb, K. Fostiropoulos, and D. R. Huffman, *ibid.* **347**, 354 (1990).

²A. F. Hebard, M. J. Roseinsky, R. C. Haddon, D. W. Murphy, S. H. Glarum, T. T. M. Palstra, A. P. Ramirez, and A. R. Kortan, *Nature (London)* **350**, 600 (1991); K. Holzer, O. Klein, S.-M. Huang, R. B. Kaner, K.-J. Fu, R. L. Whetten, and F. Diederich, *Science* **252**, 1154 (1991); H. W. Kroto, J. R. Heath, S. C. O'Brien, R. F. Curl, and R. E. Smalley, *Nature (London)* **318**, 162 (1985).

³S. Chakravarty, M. Gelfand, and S. Kivelson, *Science* **254**, 970 (1991); S. Chakravarty and S. Kivelson, *Europhys. Lett.* **16**, 751 (1991); R. W. Lof, M. A. van Veenendaal, B. Koopmans, H. T. Jonkman, and G. A. Sawatzky, *Phys. Rev. Lett.* **68**, 3924 (1992).

⁴S. R. White, S. Chakravarty, M. P. Gelfand, and S. A. Kivelson, *Phys. Rev. B* **45**, 5062 (1992).

⁵G. Stollhoff, *Phys. Rev. B* **44**, 10 998 (1991).

⁶D. Coffey and S. A. Trugman, *Phys. Rev. Lett.* **69**, 176 (1992).

⁷D. Coffey and S. A. Trugman, *Phys. Rev. B* **46**, 12 717 (1992).

⁸L. Bergomi, J. P. Blaizot, Th. Jolicœur, and E. Dagotto, *Phys. Rev. B* **47**, 5539 (1993).

- ⁹F. Willaime and L. M. Falicov, *J. Chem. Phys.* **98**, 6369 (1993).
- ¹⁰P. Joyes and R. J. Tarento, *Phys. Rev. B* **45**, 12 077 (1992).
- ¹¹P. Joyes, R. J. Tarento, and L. Bergomi, *Phys. Rev. B* **48**, 4855 (1993).
- ¹²R. T. Scalettar, A. Moreo, E. Dagotto, L. Bergomi, T. Jolicœur, and H. Monien, *Phys. Rev. B* **47**, 12 316 (1993).
- ¹³V. Elser and R. C. Haddon, *Nature (London)* **325**, 792 (1987); R. B. Mallion, *ibid.* **325**, 760 (1987); E. Manousakis, *Phys. Rev. B* **144**, R10 991 (1991); **48**, 2024 (1993).
- ¹⁴See, for instance, J. A. Vergés, E. Louis, P. S. Lommdahl, F. Guinea, and A. R. Bishop, *Phys. Rev. B* **43**, 6099 (1991); J. A. Vergés, F. Guinea, and E. Louis, *ibid.* **46**, 3562 (1992).
- ¹⁵L. M. Falicov and R. H. Victora, *Phys. Rev. B* **30**, 1695 (1984).
- ¹⁶F. López-Urias and G. M. Pastor, *Phys. Rev. B* **59**, 5223 (1999).
- ¹⁷L. M. Falicov and R. A. Harris, *J. Chem. Phys.* **51**, 3153 (1969); S. L. Reindl and G. M. Pastor, *Phys. Rev. B* **47**, 4680 (1993).
- ¹⁸See, for example, G. M. Pastor, R. Hirsch, and B. Mühlischlegel, *Phys. Rev. B* **53**, 10 382 (1996); and Ref. 16.